



Effect of Pr³⁺ Addition on the Electrical Properties of 0.94(Bi_{0.5}Na_{0.5})TiO₃-0.06(Ba_{0.9}Ca_{0.1})TiO₃ Ceramic Obtained by Pechini Method

Eric Villanueva-Vega¹ · Emilio Pradal-Velázquez^{2,3} · Federico González⁴ · Rodrigo Vivar-Ocampo¹ · Gerardo-César Díaz-Trujillo⁵ · Armando Reyes-Montero³

Received: 5 December 2022 / Accepted: 25 April 2023 / Published online: 26 May 2023
© The Author(s) 2023

Abstract

The influence of Pr³⁺ addition on the structure and electrical properties of (Bi,Na)TiO₃-(Ba,Ca)TiO₃ solid solution was investigated. In this work, 0.94(Bi_{0.5-x}Na_{0.5})TiO₃-0.06(Ba_{0.9}Ca_{0.1})TiO₃:xPr³⁺ (BNBCT6:xPr) with $x = 0, 0.1, 0.3, 0.5,$ and 0.7 mol% ceramics were prepared via a polymeric complex synthesis (Pechini method). Optimal sintering parameters were chosen in order to obtain dense ceramic microstructures. X-ray diffraction confirmed the presence of a perovskite-like structure in all the synthesized powders and sintered samples. As Pr³⁺ content increased, a large reduction in grain size was observed. BNBCT6:xPr ceramics showed a phase transition from the field-induced ferroelectric to the relaxor phase at ~ 110 °C and a local maximum around 250 °C. Dielectric permittivity was reduced as Pr³⁺ doping increased. For $x = 0.5$ mol%, maximum piezoelectric values ($d_{33} = 115$ pC/N, $-d_{31} = 27$ pC/N, $k_p = 25\%$, and $k_t = 34\%$) were obtained, while for $x = 0.7$ mol%, ferroelectric characteristics ($P_r = 14$ $\mu\text{C}/\text{cm}^2$, and $E_c = 34.7$ kV/cm) were enhanced. Bulk conductivities extracted from the impedance spectra for BNBCT6:xPr were low, consistent with the insulating characteristic of (Bi,Na)TiO₃. The achieved electrical properties suggest that BNBCT6:xPr ceramics are a potential candidate for energy transition applications.

Keywords Sodium-bismuth titanate · piezoelectric · ferroelectric · rare earth cation

Introduction

Piezoelectric and ferroelectric ceramics, with high strain and energy storage and transition capacity, have been fundamental components for developing optimal electronic devices. In this context, the properties of any functional ceramics are normally related to several aspects, such as the particle size from starting precursors, processing temperatures, morphology of the sintered products, and the stoichiometric relationship of the desired compositions.¹ Lead zirconate titanate (PZT)-based electroceramics, formulated close to the morphotropic phase boundary (MPB; a composition-dependent change of the crystal symmetry), have been the most widely used piezo/ferroelectric materials due to their excellent electric performance.² However, high lead toxicity towards the environment and human health has promoted a continuous search for eco-friendly ceramics alternatives. Bismuth-based materials, in lead-free ceramic systems, are promising candidates for diverse piezo/ferroelectric purposes as they exhibit an interesting relationship between the structure, composition, and its final electrical response.³

✉ Armando Reyes-Montero
arremo@materiales.unam.mx

¹ Facultad de Ciencias de la Ingeniería y Tecnología, Universidad Autónoma de Baja California, Tijuana, Baja California, Mexico

² Facultad de Química, Universidad Nacional Autónoma de México, 04510 Ciudad Universitaria, CDMX, Mexico

³ Instituto de Investigaciones en Materiales, Universidad Nacional Autónoma de México, 04510 Ciudad Universitaria, CDMX, Mexico

⁴ Departamento de Ingeniería de Procesos e Hidráulica, Universidad Autónoma Metropolitana-Iztapalapa, A. P. 55-534, CDMX, Mexico

⁵ Facultad de Ciencias Químicas e Ingeniería, Universidad Autónoma de Baja California, Tijuana, Baja California, Mexico

(Bi_{0.5}Na_{0.5})TiO₃ (BNT)-based solid solutions (especially for BNT-rich compositions) exhibit a ferroelectric polymorphic phase coexistence through the MPB, which are stable at each side of the boundary. The electrical properties of the material are improved in this region because of the redirection of the spontaneous polarization vector with the application of an external electric field. In particular, the (1-x)Bi_{0.5}Na_{0.5}TiO₃-xBaTiO₃ (BNT-xBT) solid solution has been of special interest due to its reported MPB between the rhombohedral (*R3c*) and the tetragonal (*P4mm*) (R-T) phases, from *x* between 0.06 and 0.07.^{4–6} Ba²⁺ cation promotes the tilting of the TiO₆ octahedra, affecting the local environment of the A-site cations by distorting the octahedra or changing the polar displacements of Ti⁴⁺ at the B-site.⁷ Moreover, relatively good piezoelectric properties with an optimum piezoelectric coefficient, *d*₃₃, a planar coupling factor, giant strain, and a pinched P–E loop have been reported for the *x* = 0.06 composition.^{8,9} The application of an intense electric field improves only textured *R3c* symmetry.⁷

Lead-free piezo/ferroelectric materials, co-doped with rare-earth cations, are frequently used to improve the electrical activity and to expand the multifunctionality of ceramics physical properties.¹⁰ For selecting the appropriate trivalent cationic species, three important physicochemical factors must be considered: (1) the stability of the perovskite phase, (2) the ionic radius, and (3) the Curie–Weiss temperature.¹¹ Among different trivalent rare-earth lanthanides, praseodymium (Pr³⁺) satisfies all three criteria.¹² In BNT-based ceramics, doping the A-site cation with a trivalent rare earth facilitates the formation of A-site vacancies, therefore enhancing local polarization,^{13,14} benefiting the piezoelectric activity in the material.^{15,16}

The volatilization of Bi₂O₃ and Na₂O, in BNT-based ceramics is often unavoidable in solid-state processing methods, due to the elevated temperatures in the calcination and densification processes.^{17,18} Generally, an excess amount of the synthesis powder is used to cover the green pellet during the sintering process to minimize the potential loss of volatile compounds. As an alternative, the Pechini method has recently been used to obtain BNT-based ceramics at lower temperatures, thus reducing the risk of compositional changes.^{6,19} This technique is based on the formation of a complex ring-shaped compound around metal cations (chelation process) with a poly-functional organic acid (e.g. citric acid). Then, as the solution is heated and a poly-hydroxyl alcohol (commonly ethylene glycol) is added, polymerization occurs, resulting in a solid polymeric resin. Eventually, the obtained product is decomposed, normally at temperatures between 500 °C and 800 °C, producing a very fine ceramic powder. Therefore, compared with the conventional solid-state method, wet chemical routes such as the Pechini method, emulsion method, citrate method, and sol–gel method, exhibits some advantages, such as

compositional homogeneity, excellent chemical stoichiometry, and a low crystallization temperature.¹⁹

Currently, it is known that BNT ceramics stand out for their high polarization; however, their large hysteresis and low breakdown strength lead to low energy storage density and large energy loss. With the incorporation of different lead-free perovskite-type materials, such as SrZrO₃, NaNbO₃, and BaTiO₃ (BT), it is possible to stabilize the phase structure, diminish the hysteresis, enhance the breakdown strength of ferroelectric ceramics, and reduce the phase transition temperature.^{20–22} This results in BNT-based solid solutions for energy storage applications, high-temperature stability against temperature and frequency, and actuator applications. In BNT-BT ceramics, the incorporation of Ca²⁺ in the vicinity of the MPB results in lattice distortions, disruption of polar nano-regions (PNRs), and the weakening of the ferroelectric coupling behavior, which are ideal characteristics for a ceramic material with enhanced dielectric properties.^{23,24} Additionally, the effect on the electrical properties of (1-x)Bi_{0.5}Na_{0.5}TiO₃-(x)Ba_(1-y)Ca_(y)TiO₃ (BNT-xBCT) solid-solution, incorporating rare-earth cations has not yet been explored.

In this work, 0.94(Bi_{0.5-x}Na_{0.5})TiO₃-0.06(Ba_{0.9}Ca_{0.1})TiO₃:xPr³⁺ (BNBCT6:xPr) ceramics with *x* = 0, 0.1, 0.3, 0.5, and 0.7 mol% were synthesized via the Pechini method. The effect that Pr³⁺ has on the structure/microstructure and electrical properties of the material has been systematically investigated. This work attempts to correlate the synthesis route with the optimum piezo/ferroelectric properties development, which are important parameters for assessing the electrical performance of multifunctional ceramics.

Experimental

BNBCT6:xPr (*x* = 0, 0.1, 0.3, 0.5 and 0.7 mol%) powders were synthesized via the polymeric precursor method. A Ti solution was prepared by dissolving Ti[OCH(CH₃)₂]₄ (Sigma-Aldrich, 97%) in anhydrous ethyl alcohol (J.T. Baker, 99.9%) with citric acid C₃H₄(COOH)₃ (Sigma-Aldrich, 99.5%). Two further solutions were prepared by dissolving Ba(NO₃)₂ (Sigma-Aldrich, 99%) and Na(NO₃)₂·4H₂O (99.8%) in deionized water, and Bi(NO₃)₃·5H₂O and Ca(NO₃)₂·4H₂O in ethylene glycol (Sigma-Aldrich, 99%). These two solutions were poured into the first one. Ethylene glycol and citric acid were used in a 4:1 M ratio. The final solution was stirred and heated to 90°C until it gradually became transparent. Next, the temperature was raised to 120°C and, after 24 h, it became a dark brown glassy resin. This resin was pre-calcined at 300°C for 1 h, obtaining a solid black material which was ground into a granulated powder with an agate mortar. The powder was then calcined at 800°C in air for 1 h and ball-milled for 10 h using zirconia

ball media and ethanol. Then, it was dried and pressed into pellets of 13.0 mm diameter and sintered at 1100 °C for 2 h. The experimental density, from the sintered pellets, was measured by the Archimedes method.

The crystal structure of the BNBCT6:*x*Pr (*x* = 0, 0.1, 0.3, 0.5, and 0.7 mol%) powders and sintered samples were examined using X-ray diffraction (XRD) with a Cu α_1 radiation (1.54178 Å; D8 Advance Lynx eye detector; Bruker). Data was collected from 20° to 80° (in two-theta range) using 40 kV and 40 mA in the x-ray generator. The morphology of the dense ceramic samples, previously sputter-coated with Au/Pd was observed by a field-emission scanning electron microscope (7600f; JEOL), and further analyzed by computer-aided image analysis software (Image J). The average grain size of a large sample area was determined by the interception method. The elemental composition of the ceramics was determined by an energy dispersive spectrometry (EDS) analysis, and the EDS spectra were acquired and treated using INCA software (Oxford Instruments).

In order to measure the electrical properties, the sintered ceramics were polished. Then, both circular faces were coated with Ag and annealed at 600 °C for 30 min. For piezoelectric evaluation, the sintered ceramics were poled under a 4 kV/mm DC field at room temperature in a silicon oil bath. The dielectric permittivity (ϵ_{33}^T) and losses ($\tan \delta$) were measured with a precision impedance analyzer (4294A; Agilent) before and after poling. The piezoelectric constant d_{33} was measured after 24 h of the poling process using a d_{33} -PiezoMeter System (Piezotest). Dielectric permittivity (at the resonance frequency), piezoelectric coefficients (d_{31} , e_{33} , and h_{33}), as well as the electromechanical coupling factors k_i and the elastic stiffness c_{ij} for the radial and thickness modes

were calculated using an automated iterative method.²⁵ Ferroelectric hysteresis loops were measured at room temperature using a ferroelectric workstation (RT66b; Radiant Technologies) at 10 Hz.

To determine the bulk conductivities, impedance spectra data was collected between 100 mHz and 1 MHz, with an applied voltage of 100 mV using a frequency response analyzer (1260; Solartron) connected to a dielectric interface (1296A; Solartron) in a temperature range from 400 °C to 900 °C with steps of 25 °C.

Results and Discussion

Structure and Microstructure

Figure 1a shows the XRD patterns of the BNBCT6:*x*Pr (*x* = 0, 0.1, 0.3, 0.5, and 0.7 mol%) powders calcined at 800 °C for 1 h. All the samples exhibit a typical perovskite-like structure with no traces of secondary phase, suggesting that BCT and Pr³⁺ were incorporated into the BNT lattice to form a solid solution. It is worth noticing that the XRD maxima of the BNBCT6:*x*Pr powders slightly shift to lower angles as the Pr³⁺ content increases (Fig. 1b), suggesting that the crystal lattice only expands its dimensions while maintaining the crystal symmetry. The ionic radius of Pr³⁺ is smaller than that of Bi³⁺, so these results are compatible with the substitution of Bi³⁺ by Pr³⁺. Considering that the lattice can contract around vacancies, a likely possibility is that, since Pr₂O₃ is less volatile than Bi₂O₃, substituting Bi³⁺ for Pr³⁺ results in fewer A-site and oxygen vacancies and the cell becomes larger with higher Pr³⁺ content within the

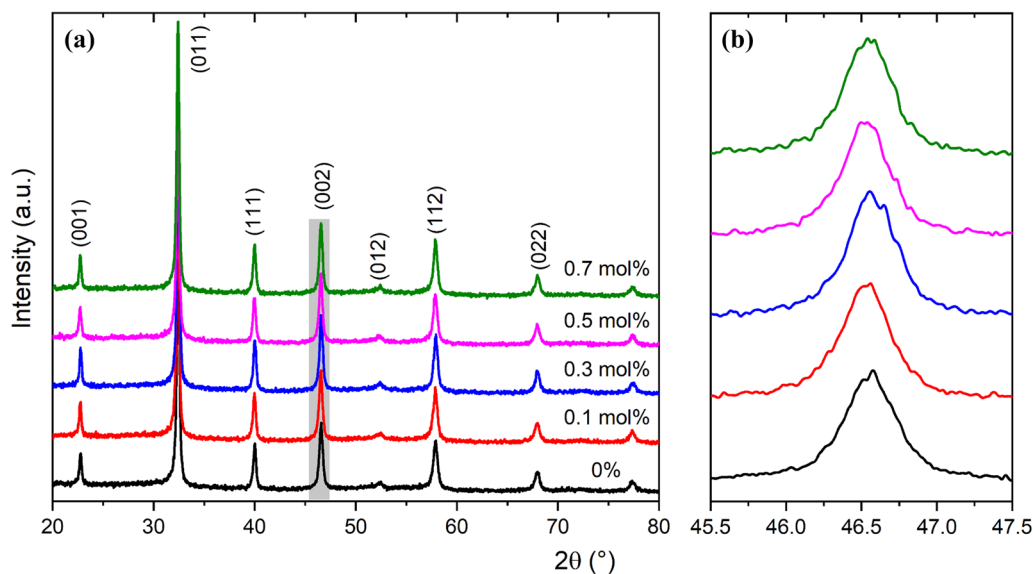


Fig. 1 (a) XRD patterns of BNBCT6:*x*Pr calcined powders at 800 °C for 1 h, (b) magnification around the (002) diffraction peak.

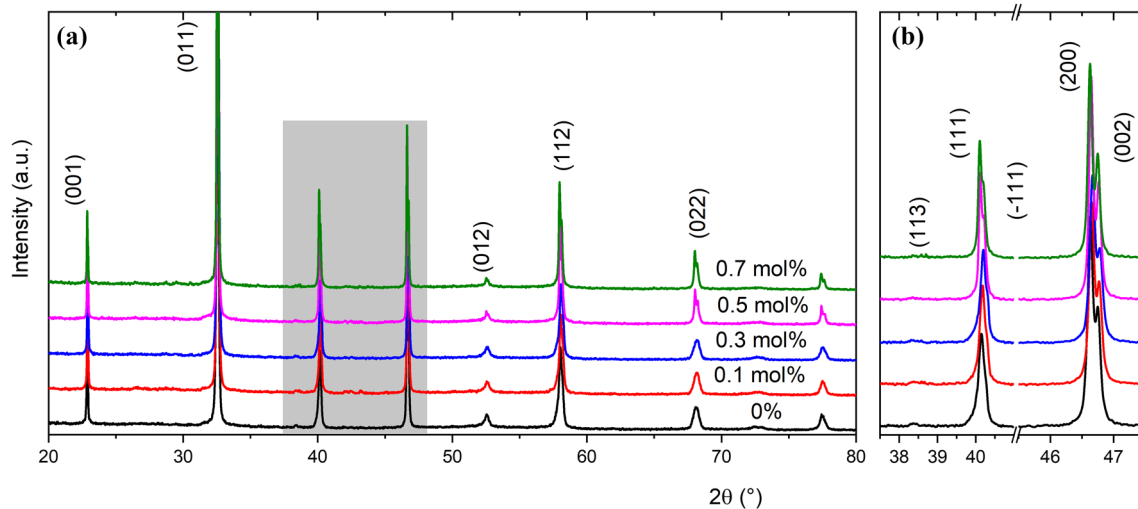


Fig. 2 (a) XRD patterns of BNBCT6:*x*Pr ceramics sintered at 1100 °C for 2 h, (b) magnification in 2θ between 37.5° and 47.5°.

Table I Calculated grain size and density for BNBCT6:*x*Pr samples ($x = 0, 0.1, 0.3, 0.5, 0.7$ mol%)

Sample (mol%)	Grain size (μm)	Calculated density (g/cm ³)	Average measured density (g/cm ³)	Ceramics Densification (%)
0	1.16 ± 0.56	5.98	5.75	96
0.1	1.56 ± 0.29	5.98	5.63	94
0.3	1.30 ± 0.27	5.98	5.68	95
0.5	1.06 ± 0.23	5.98	5.70	95
0.7	0.93 ± 0.28	5.98	5.72	96

concentrations explored. The obtained XRD patterns were indexed to the perovskite-like cubic prototype structure.

Figure 2a displays the XRD patterns of the BNBCT6:*x*Pr ($x = 0, 0.1, 0.3, 0.5,$ and 0.7 mol%) sintered ceramics at 1100 °C for 2 h. For a better phase identification, selected 2θ angles in the range of 37–42° and 45.5–47.5° were enlarged, as seen in Fig. 2b. In BNT-BT-based solid solutions, the coexistence of rhombohedral $R3c$ and tetragonal $P4mm$ symmetries occurs at the edge of the MPB. This fact gives place to the 111 and 002 cubic prototype peaks splitting and the emergence of the 113 peak, at the low-angle side of the 111 doublet.^{6,26} In this work, as the Pr³⁺ content increases, the splitting of the 111/-111 and 002/200 diffraction peaks becomes more evident (Fig. 2b), and could be attributed to the rhombohedral polar phase and the tetragonal weakly polar phase, respectively. Calculated density, from the diffraction patterns of the BNBCT6:*x*Pr sintered ceramics, is shown at Table I.

SEM micrographs for BNBCT6:*x*Pr ($x = 0, 0.1, 0.3, 0.5,$ and 0.7 mol%) sintered samples are shown in Fig. 3. Fully dense microstructures with well-grown grains, without any

apparent secondary phase, were obtained. All the sintered samples exhibited pseudocubic-shaped particles. In the BNBCT6:*x*Pr sample with $x = 0\%$ (Fig. 3a), an irregular microstructure is observed, unlike samples doped with Pr³⁺ (Fig. 3b–e), in which a more homogenous microstructure distribution was achieved. In order to analyze the elemental composition of the different sized grains obtained in the BNBCT6:*x*Pr sample with $x = 0$ mol%, EDS spectra was collected (Fig. 4). The chemical composition between smaller (Fig. 4b) and larger grains (Fig. 4c) confirmed no apparent differences. Furthermore, Table I displays the measured density and the grain size for undoped/doped-Pr³⁺ ceramics. It is noticed that grain size reduces as the calculated density increases with Pr³⁺ content. The reduction in grain size agrees with previous reports^{27,28} noticing that rare-earth elements act as a pinning agent, leading to the inhibition of grain boundary diffusion. In Pr-doped BNT, Pr³⁺ acts as an inhibitor during the grain growth process due to the lower diffusion rate.²⁹

Electrical Evaluation

Dielectric Analysis

The dielectric permittivity (ϵ_r) and dielectric loss ($\tan \delta$), as a function of temperature, for the BNBCT6:*x*Pr samples are shown in Fig. 5. For the $x = 0$ mol% sample, a very sharp increase in permittivity around 110°C and a local maximum of the permittivity around 250 °C (maximum permittivity, T_m) are observed (Fig. 5a). T_m represents the relaxation temperature of the rhombohedral–tetragonal transition by showing a slight frequency dependence produced from a fraction of the PNRs.^{30,31} The observed relaxor behavior is attributed to the structural disordering in the arrangement

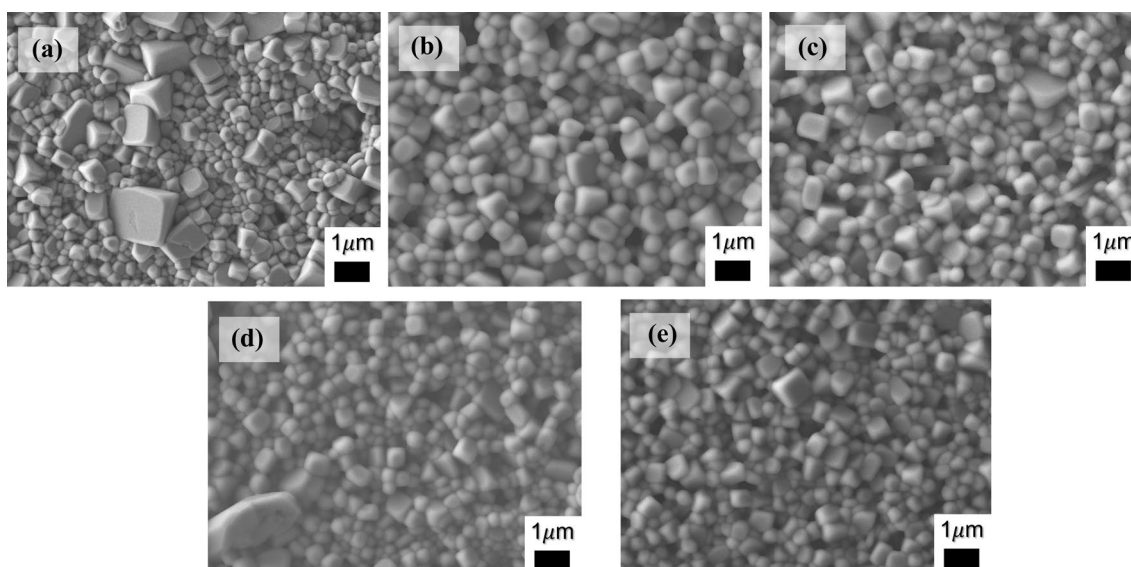


Fig. 3 SEM images of BNBCT6: x Pr ceramics sintered by a conventional high-temperature process at 1100 °C: (a) 0, (b) 0.1, (c) 0.3, (d) 0.5, and (e) 0.7 mol%.

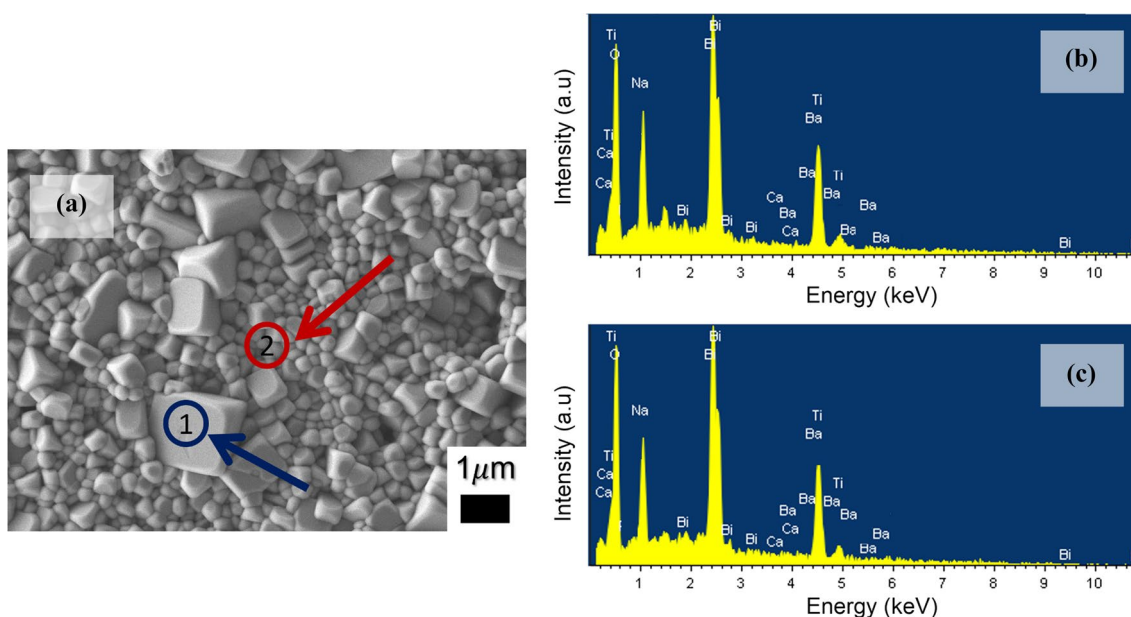


Fig. 4 (a) SEM image of BNBCT6: x Pr ($x = 0$ mol%) ceramic where cubic and spherical shapes are identified as 1 and 2, respectively. EDS spectra of (b) smaller and (c) larger grains show peaks for barium, calcium, bismuth, sodium, titanium, and oxygen.

of the A-site cations and the compositional fluctuation.³² Figure 5b reveals that dielectric losses are below 0.1% near T_m . As can be seen, for $x = 0.3$ mol%, the dielectric permittivity is enhanced (near room temperature); however, as the Pr^{3+} content increases, the dielectric permittivity reduces (Fig. 5c). For all the BNBCT6: x Pr samples, a dielectric broad-like behavior is present with a low dielectric loss response (below 0.1%; Fig. 5d).

Piezoelectric Analysis

Complex impedance spectra for the fundamental radial and thickness modes (from a thickness poled BNBCT6: x Pr $x = 0.5\%$ mol ceramic disc) are shown in Fig. 6. The real part of the complex impedance (resistance, R) and the real part of the complex admittance (conductance, G) are an alternative representation of the

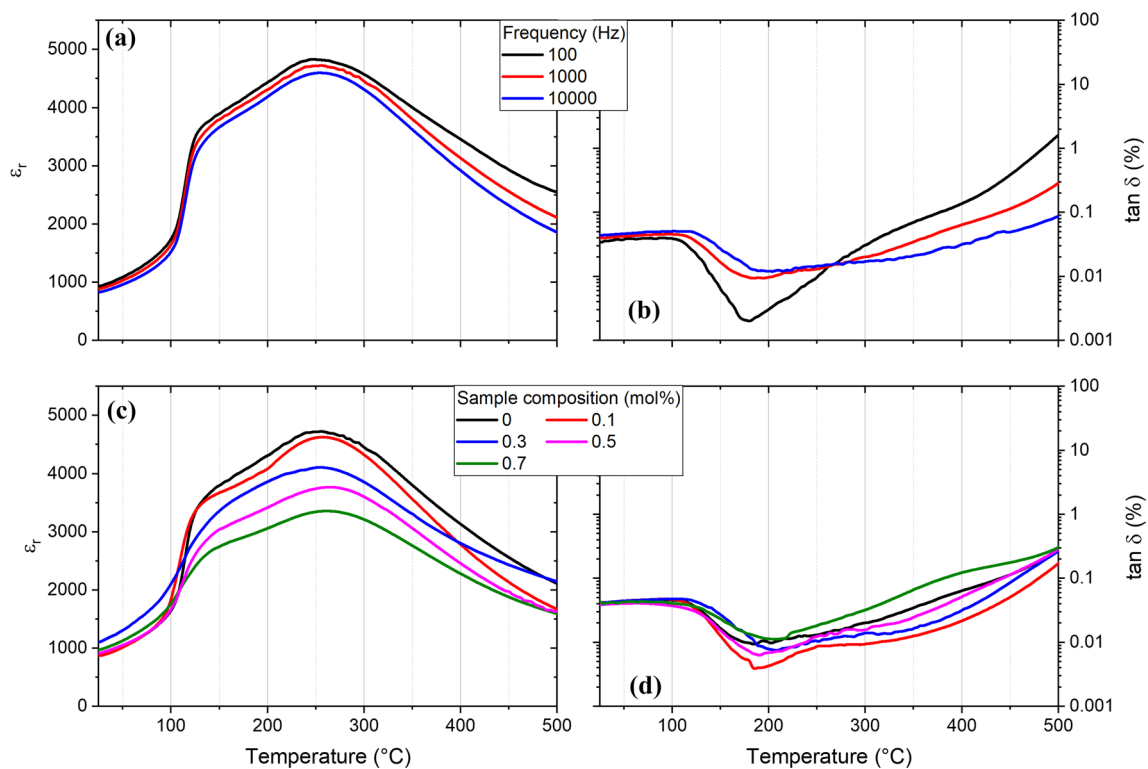


Fig. 5 (a) Dielectric permittivity and (b) dielectric loss for BNBCT6:*x*Pr (*x* = 0 mol%) at different frequencies. Comparison between (c) dielectric permittivity and (d) dielectric loss for doped and undoped sintered BNBCT6:*x*Pr samples at 1 kHz.

modulus and phase angle (see supplementary Figure S1). This type of plot has been selected to allow the automatic determination of the frequencies of the maximum *G* and *R* values.³³ Additionally, in Fig. 6a and b, the reconstructed spectra carried by the insertion of the calculated material coefficients in the expression of the complex impedance versus frequency for each given resonance are indicated. The accuracy of this reconstruction, characterized by the regression factor (R^2) of the reconstructed to the experimental peaks, is considered as a quality test of the material parameters.³⁴ The higher validity of the R^2 coefficients (~ 1) is elevated in both considered resonances (Table II).

Elastic compliance (s_{ij}^*) and stiffness (c_{ij}^*) constants, as well as dielectric permittivity and piezoelectric coefficients, were calculated from the frequency dependence of the complex impedance (Table II) by an automatic iterative method.²⁵ Electromechanical coupling factors (k_i) and frequency numbers (N_i) were also determined. This set of calculated parameters includes the three types of losses: dielectric, piezoelectric, and elastic. The highest k_p was observed on the BNBCT6:*x*Pr ceramic sample with *x* = 0.5 mol%, suggesting that the highest piezoelectric constants ($-d_{31}$ and d_{33}) are expected for this composition.

This condition is attributable to the MPB and fine microstructure which enables easy poling. Additionally, the inclusion of Pr³⁺ ions into the A site of the perovskite reduces the pinning of domains and facilitates domain wall motion.³⁵

Ferroelectric Analysis

In order to understand the relationship between the physical–chemical phenomena associated with the building-up of a macroscopic polarization and the electromechanical properties of this material, the electric field dependence of polarization (*P*–*E* loops) as a function of the applied voltage and concentration were measured at room temperature (Fig. 7). Saturated and square-like loops were obtained for all the BNBCT6:*x*Pr ceramics (Fig. 7a). It is known that lower values of the coercive field (E_c) make the poling more efficient, while larger values of the remanent polarization (P_r) favor the piezoelectric activity.³⁶ In the obtained ceramics, the maximum measured values for P_r (14 $\mu\text{C}/\text{cm}^2$) and E_c (34.7 kV/cm) are for *x* = 0.7 mol%, while for *x* = 0.5 mol%, maximum polarization (P_{max}) and capacitance (*C*) were achieved (Fig. 7b and c). This result is in accordance with the reported piezoelectric activity. Further work on XRD as a function of the electric field

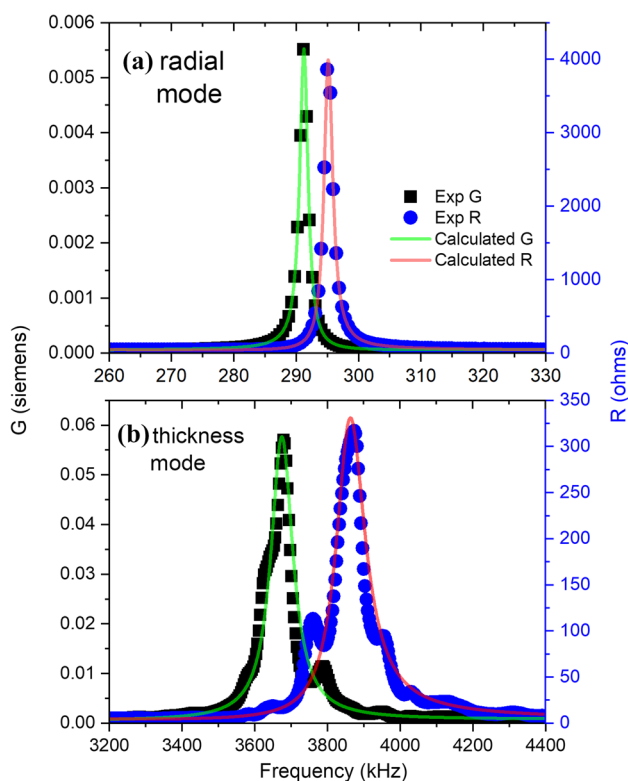


Fig. 6 Experimental and reconstructed spectra after parameter determination, by the iterative analysis of the complex impedance (a) radial and (b) thickness modes extension of a thickness poled thin disc.

will be necessary to clarify the importance of the field-induced structural transition in the MPB regimes of the polarization building.

Electrical Conductivity

Impedance spectroscopy can separate the contributions of different regions in the sample (i.e. bulk, grain boundaries, electrodes) from the total electrical response. The product of the resistance (R) and capacitance (C) for each region defines the time constant for that region, and its reciprocal is the angular frequency (ω) at which certain features appear. Impedance data can be presented and analyzed through 4 interrelated formalisms:

$$\text{Impedance } Z^* = Z' - jZ'' \quad (1)$$

$$\text{Admittance } Y^* = 1/Z^* = Y' + jY'' \quad (2)$$

$$\text{Electric modulus } M^* = j\omega C_0 Z^* = M' + jM'' \quad (3)$$

$$\text{Permittivity } \epsilon^* = 1/M^* = \epsilon' - j\epsilon'' \quad (4)$$

The impedance of each region in the sample can, in principle, be modeled with a parallel RC element. For each RC element connected in series, a semicircle is expected in the Z^* and M^* plots with its maximum occurring at the frequency defined by its time constant. In the Z'' and M'' spectroscopic plots, each RC element is expected to give rise to a Debye peak centered at frequency ω , although how distinguishable they are, depends on the characteristics of that element and the formalism that is being analyzed. For example, the M'' plots give more weight to the responses that appear at higher frequencies and have lower capacitances (such as the bulk); a high capacitance response occurring at low frequencies is not often seen in M'' spectra. The height of a Debye peak in a M'' spectrum corresponds to $\frac{1}{2}\epsilon_r$, and it is centered at a frequency (f) such as $2\pi fRC = 1$, so both the capacitance and resistance of that element can be extracted from the Debye peak. Similarly, they can be extracted from Debye peaks in Z'' spectra, where the peak maximum corresponds to $R/2$.

Figure 8 shows the Z^* (Fig. 8a) and M'' and Z'' spectroscopic plots (Fig. 8b) for the BNBCT6: x Pr ceramics with $x = 0.7$ mol%. At lower temperatures, two electrical responses may be distinguished for all the BNBCT6: x Pr samples in the M'' spectra (except for the one with $x = 0.5$ mol%) in which the lower frequency has a smaller capacitance (3.7×10^{-11} to 4.9×10^{-10} F cm $^{-1}$) and is attributed to the bulk. The higher frequency response has capacitances that diminish with temperature (in the measured temperature range) and vary from 1.8×10^{-10} to 1.7×10^{-9} F cm $^{-1}$, which could be attributed to undetected secondary phases or to BNT grains with a slightly different composition but noticeably different electrical conductivity. The capacitances extracted from the M'' spectra for these two responses in the sample with $x = 0.7$ mol% are shown in supplementary Figure S2. The larger grains observed in the micrographs (Fig. 4) could be more conductive BNT grains that formed slightly Barich (the difference in composition could be lower than the sensitivity in EDS) and are acceptor-doped.³⁷ For most samples, this response cannot be well resolved from the bulk response above a certain temperature (between 375 and 450 °C). At higher temperatures, an additional low-frequency response is seen in the Z^* and Z'' plots, with capacitances ranging from 5.7×10^{-7} to 9.6×10^{-6} F cm $^{-1}$. This could have originated from the surface of the grains or the sintered pellets. Bulk conductivities, extracted from M'' peaks, are presented as an Arrhenius plot in Fig. 9, and the conductivities are low, consistent with insulating-type BNT (type III: dielectric BNT with low electrical—mostly electronic—conductivity and low dielectric losses).¹⁷ The activation energies range between 1.42 and 1.65 eV, these values being close to half of the band gap in BNT,³⁸ therefore indicating that the low conductivity

Table II Piezoelectric coefficients obtained for BNBCT6:xPr ceramics for radial and thickness modes

Sample (mol%)	Elastic compliance constants: $s_{ij}^* = (s_{ij})_{\text{real}} + i(s_{ij})_{\text{img}}$ [10^{-12} m ² /N]				
	s_{11}^E	s_{12}^E	s_{66}^E	s_{11}^D	s_{12}^D
0	8.50 – 0.04 <i>i</i>	– 2.73 + 0.01 <i>i</i>	22.45 – 0.10 <i>i</i>	8.36 – 0.04 <i>i</i>	– 2.86 + 0.01 <i>i</i>
0.1	8.78 – 0.04 <i>i</i>	– 2.19 + 0.01 <i>i</i>	21.94 – 0.10 <i>i</i>	8.65 – 0.04 <i>i</i>	– 2.32 + 0.01 <i>i</i>
0.3	8.76 – 0.04 <i>i</i>	– 2.50 + 0.01 <i>i</i>	22.52 – 0.10 <i>i</i>	8.62 – 0.04 <i>i</i>	– 2.64 + 0.01 <i>i</i>
0.5	8.39 – 0.05 <i>i</i>	– 2.23 + 0.01 <i>i</i>	21.24 – 0.12 <i>i</i>	8.29 – 0.05 <i>i</i>	– 2.33 + 0.01 <i>i</i>
0.7	8.77 – 0.05 <i>i</i>	– 2.67 + 0.01 <i>i</i>	22.89 – 0.12 <i>i</i>	8.64 – 0.04 <i>i</i>	– 2.81 + 0.01 <i>i</i>
Sample (mol%)	Elastic stiffness constants $c_{ij}^* = (c_{ij})_{\text{real}} + i(c_{ij})_{\text{img}}$ [10^{-12} N/m ²]				
	c_{11p}^E	c_{11p}^D	c_{33}^E	c_{33}^D	
0	13.12 + 0.06 <i>i</i>	13.55 + 0.06 <i>i</i>	16.75 + 1.20 <i>i</i>	20.57 + 1.60 <i>i</i>	
0.1	12.13 + 0.06 <i>i</i>	12.47 + 0.05 <i>i</i>	13.21 + 0.60 <i>i</i>	15.66 + 0.48 <i>i</i>	
0.3	12.43 + 0.05 <i>i</i>	12.79 + 0.05 <i>i</i>	14.21 + 0.56 <i>i</i>	17.65 + 0.52 <i>i</i>	
0.5	12.83 + 0.07 <i>i</i>	13.11 + 0.07 <i>i</i>	14.38 + 0.27 <i>i</i>	16.22 + 0.41 <i>i</i>	
0.7	12.56 + 0.06 <i>i</i>	12.94 + 0.07 <i>i</i>	14.80 + 1.01 <i>i</i>	18.45 + 1.43 <i>i</i>	
Sample (mol%)	Piezoelectric coefficients				
	[10^{-12} N/C]		[10^{-3} Vm/N]	[10^8 V/m]	[C/m ²]
	$-d_{31}$	d_{33}^a	$-g_{31}$	h_{33}	e_{33}
0	25.25 – 0.61 <i>i</i>	100	5.34 + 0.08 <i>i</i>	34.74 + 1.65 <i>i</i>	11.02 + 0.64 <i>i</i>
0.1	23.98 – 0.56 <i>i</i>	102	5.80 + 0.07 <i>i</i>	28.89 – 0.27 <i>i</i>	8.50 – 0.35 <i>i</i>
0.3	23.08 – 0.54 <i>i</i>	105	5.89 + 0.05 <i>i</i>	37.52 + 0.23 <i>i</i>	9.17 – 0.15 <i>i</i>
0.5	27.17 – 0.59 <i>i</i>	115	5.55 + 0.13 <i>i</i>	32.76 + 1.52 <i>i</i>	8.09 + 0.06 <i>i</i>
0.7	25.60 – 0.64 <i>i</i>	109	5.24 + 0.12 <i>i</i>	34.96 + 2.14 <i>i</i>	10.48 + 0.54 <i>i</i>
Sample (mol%)	Electromechanical coupling factors (k_{ij})[%] and frequency number (N_i) [kHz mm]				
	k_p	k_{31}	k_t	N_p	N_t
0	22	13	33	3137	2757
0.1	21	13	36	3009	2538
0.3	21	12	34	3064	2577
0.5	25	16	34	3113	2538
0.7	21	12	35	3078	2616
Sample (mol%)	Dielectric permittivity		R^2		
	ϵ_{33}^T	ϵ_{33}^S	Radial	Thickness	
0	533.41 – 20.46 <i>i</i>	358.52 – 3.86 <i>i</i>	0.9974	0.9127	
0.1	467.32 – 16.62 <i>i</i>	332.23 – 5.53 <i>i</i>	0.9944	0.9587	
0.3	442.41 – 14.50 <i>i</i>	276.03 – 6.19 <i>i</i>	0.9969	0.9585	
0.5	549.59 – 13.72 <i>i</i>	399.37 – 3.56 <i>i</i>	0.9988	0.9466	
0.7	550.74 – 25.98 <i>i</i>	338.40 – 3.27 <i>i</i>	0.9982	0.9151	

^aNot calculated from resonance data

in these samples is mostly electronic. At higher temperatures, the conductivities of the Pr-doped samples are very similar and slightly lower than the 0 mol% sample. As discussed earlier, regarding the cell expansion, the substitution of Bi³⁺ for Pr³⁺ may lead to lower concentrations of oxygen vacancies (since Pr₂O₃ is not as volatile

as Bi₂O₃), lowering the conductivity with respect to the 0 mol% sample. The insulating behavior of these samples is associated with the softer processing conditions (compared to solid-state synthesis) that avoid the formation of oxygen vacancies.³⁹

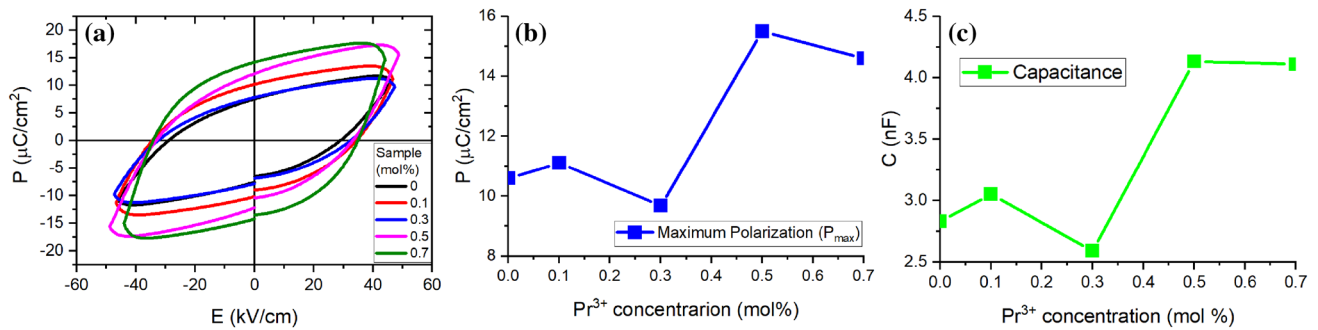


Fig. 7 (a) Ferroelectric P–E hysteresis loops for BNBCT6:*x*Pr ceramics. Evolution of (b) P_{\max} and (c) C as a function of Pr^{3+} mol concentration.

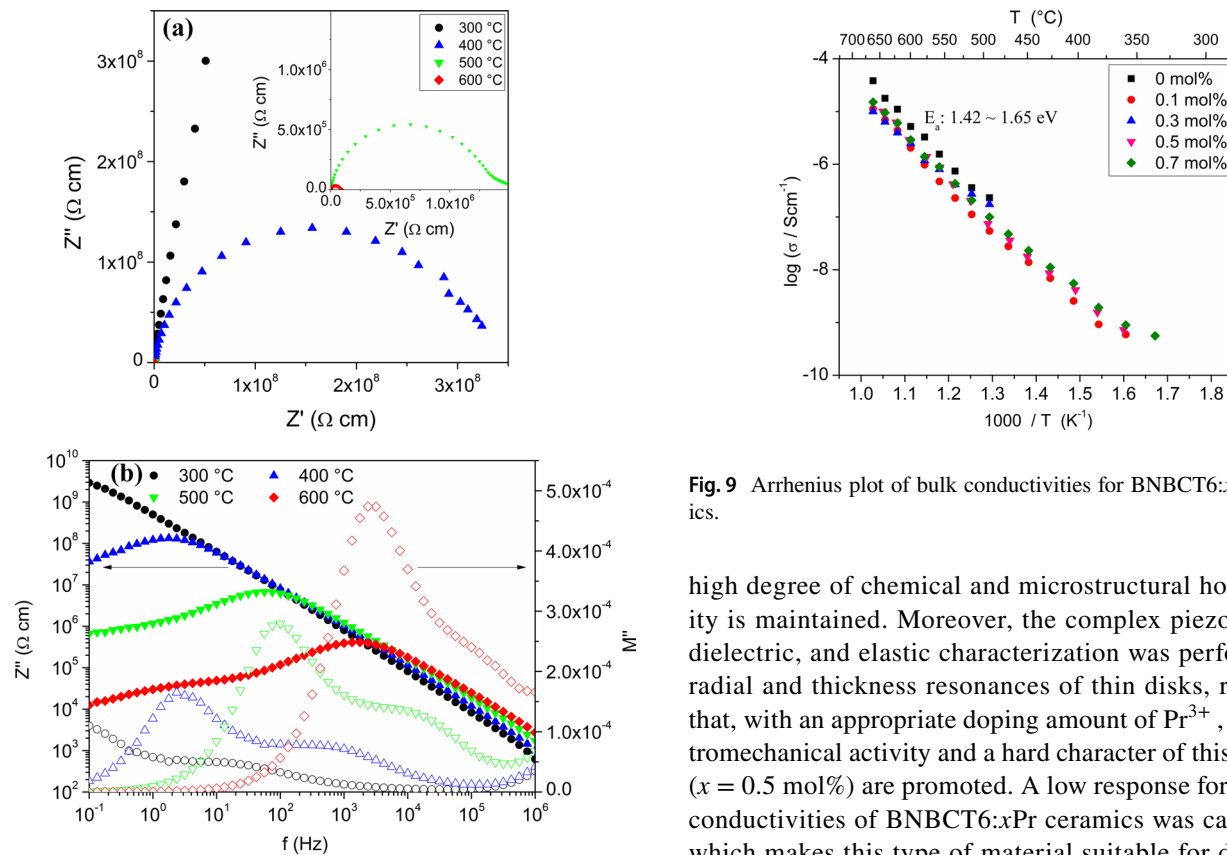


Fig. 8 (a) Z^* and (b) Z'' and M'' spectroscopic plots for BNBCT6:*x*Pr with $x = 0.7$ mol% at 300, 400, 500, and 600 °C. The inset in (a) shows the electrical response at higher temperatures.

Conclusions

Dense BNBCT6:*x*Pr ceramics with $x = 0, 0.1, 0.3, 0.5,$ and 0.7 mol% were obtained via the Pechini method. XRD patterns revealed that Pr^{3+} was introduced into the $(\text{Bi,Na})\text{TiO}_3$ - $(\text{Ba,Ca})\text{TiO}_3$ lattice to form a solid solution. The incorporation of Pr^{3+} ion reduces grain size, and a

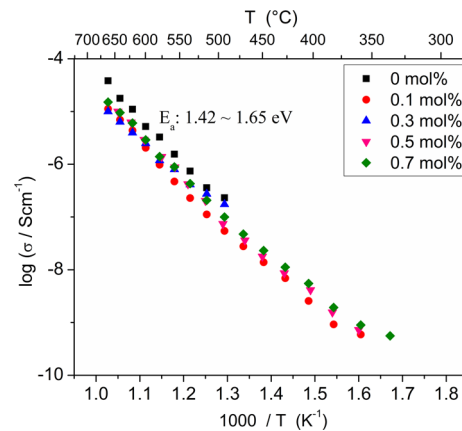


Fig. 9 Arrhenius plot of bulk conductivities for BNBCT6:*x*Pr ceramics.

high degree of chemical and microstructural homogeneity is maintained. Moreover, the complex piezoelectric, dielectric, and elastic characterization was performed at radial and thickness resonances of thin disks, revealing that, with an appropriate doping amount of Pr^{3+} , the electromechanical activity and a hard character of this ceramic ($x = 0.5$ mol%) are promoted. A low response for the bulk conductivities of BNBCT6:*x*Pr ceramics was calculated, which makes this type of material suitable for dielectric or ferroelectric applications. Compared to other lead-free-based ceramics, this BNBCT6:*x*Pr solution may facilitate the development of other structurally engineered materials (i.e., luminescent or optoelectronic) in a wide range of operating temperatures (up to 280 °C).

Supplementary Information The online version contains supplementary material available at <https://doi.org/10.1007/s11664-023-10486-8>.

Acknowledgments E. Villanueva-Vega is grateful to the Autonomous University of Baja California for the granted financial support for the research project of the Engineering and Technology in Renewable Energies academic group. A. Reyes-Montero thanks PAPIIT-UNAM (IN102622) for financial support. All authors thank DRX-lab at UAM-I (T128) for x-ray diffraction measurements and to Omar Novelo Peralta

and Lourdes Soledad Bazán Díaz (IIM-UNAM) for SEM images acquisition and technical support. E. Pradal-Velázquez thanks CONACYT for the scholarship under “Estancias Posdoctorales por México”.

Author Contributions EV-V, RV-O and AR-M conceived the idea and designed the experiments. FG and AR-M completed the structural and microstructural characterization. EP-V and AR-M performed the electrical characterization of the material. EV-V, EP-V, G-CD-T, and AR-M wrote the manuscript. All authors have read and agreed to the published version of the manuscript.

Data Availability The data that support the findings of this study are available within the supplementary material.

Conflict of interest The authors have no conflicts to disclose.

Open Access This article is licensed under a Creative Commons Attribution 4.0 International License, which permits use, sharing, adaptation, distribution and reproduction in any medium or format, as long as you give appropriate credit to the original author(s) and the source, provide a link to the Creative Commons licence, and indicate if changes were made. The images or other third party material in this article are included in the article's Creative Commons licence, unless indicated otherwise in a credit line to the material. If material is not included in the article's Creative Commons licence and your intended use is not permitted by statutory regulation or exceeds the permitted use, you will need to obtain permission directly from the copyright holder. To view a copy of this licence, visit <http://creativecommons.org/licenses/by/4.0/>.

References

- M.E. Villafuerte-Castrejón, E. Morán, A. Reyes-Montero, R. Vivar-Ocampo, J.A. Peña-Jiménez, S.O. Rea-López, and L. Pardo, Towards lead-free piezoceramics: facing a synthesis challenge. *Materials* 9, 21 (2016).
- P.K. Panda and B. Sahoo, PZT to lead free piezo ceramics: a review. *Ferroelectrics* 474(1), 128 (2015).
- X. Zhou, G. Xue, H. Luo, C.R. Bowen, and D. Zhang, Phase structure and properties of sodium bismuth titanate lead-free piezoelectric ceramics. *Prog. Mater. Sci.* 122, 100836 (2021).
- R. Machado, V.B. dos Santos, D.A. Ochoa, E. Cerdeiras, L. Mestres, and J.E. García, Elastic, dielectric and electromechanical properties of (Bi_{0.5}Na_{0.5})TiO₃-BaTiO₃ piezoceramics at the morphotropic phase boundary region. *J. Alloys Compd.* 690, 568 (2017).
- L. Pardo, A. García, K. Brebøl, E. Mercadelli, and C. Galassi, Enhanced properties for ultrasonic transduction phase transitions and thermal depoling in 0.96(Bi_{0.5}Na_{0.5})TiO₃-0.04BaTiO₃ submicrometre-structured ceramics. *J. Phys. D* 44, 335404 (2011).
- R. Vivar-Ocampo, L. Pardo, D. Ávila, E. Morán, A.M. González, L. Bucio, and M.E. Villafuerte-Castrejón, Piezoelectric ceramics of the (1-x)Bi_{0.50}Na_{0.50}TiO₃-xBa_{0.90}Ca_{0.10}TiO₃ lead-free solid solution: chemical shift of the morphotropic phase boundary, a case study for x=0.06. *Materials* 10, 736 (2017).
- J. Canche-Tello, M.E. Montero-Cabrera, M.E. Fuentes-Montero, L. Pardo, H.E. Esparza-Ponce, H. Castillo-Michel, I. Castillo-Sandoval, J.M. Nápoles-Duarte, S.D. Juárez-Escamilla, and L.E. Fuentes-Cobas, Oxygen vacancy micrometric enrichment in high-performance lead-free piezoelectric ceramic (Bi_{0.5}Na_{0.5})_{0.94}Ba_{0.06}TiO₃: a synchrotron radiation study. *J. Eur. Ceram. Soc.* 39(4), 1020 (2019).
- W. Jo, R. Ditzler, M. Acosta, J. Zang, C. Groh, E. Sapper, K. Wang, and J. Rödel, Giant electric-field-induced strains in lead-free ceramics for actuator applications—status and perspective. *J. Electroceram.* 29, 71 (2012).
- H. Simons, J.E. Daniels, J. Glaum, A.J. Studer, J.L. Jones, and M. Hoffman, Origin of large recoverable strain in 0.94(Bi_{0.5}Na_{0.5})TiO₃-0.06BaTiO₃ near the ferroelectric-relaxor transition. *Appl. Phys. Lett.* 102(6), 062902 (2013).
- C.M. Lau, X.W. Xu, and K.W. Kwok, Photoluminescence, ferroelectric, dielectric and piezoelectric properties of Er-doped BNT-BT multifunctional ceramics. *Appl. Surf. Sci.* 336, 314 (2015).
- U. Chon and J.S. Shim, Ferroelectric properties and crystal structure of praseodymium-modified bismuth titanate. *J. Appl. Phys.* 93, 4769 (2003).
- R.W. Wolfe and R.E. Newnham, Rare earth bismuth titanates. *J. Electrochem. Soc.* 116, 832 (1969).
- Y. Zhang and J.F. Li, Review of chemical modification on potassium sodium niobate lead-free piezoelectrics. *J. Mater. Chem. C* 7, 4284 (2019).
- A. Deng and J. Wu, Enhanced strain and electrostrictive properties in lead-free BNT-based ceramics via rare earth doping. *J. Mater. Chem.* 8(2), 401 (2022).
- A. Nesterović, J. Vukmirović, I. Stijepović, M. Milanović, B. Bajac, E. Tóth, Ž. Cvejić, and V. Srdić, Structure and dielectric properties of (1-x)Bi_{0.5}Na_{0.5}TiO₃-xBaTiO₃ piezoceramics prepared using hydrothermally synthesized powders. *R. Soc. Open Sci.* 8, 202365 (2021).
- T. Schulz, V. Veerapandyan, M. Deluca, and J. Töpfer, Synthesis and properties of lead-free BNT-BT-xCZ ceramics as high-temperature dielectrics. *Mater. Res. Bull.* 145, 111560 (2022).
- F. Yang, M. Li, L. Li, P. Wu, E. Pradal-Velázquez, and D.C. Sinclair, Defect chemistry and electrical properties of sodium bismuth titanate perovskite. *J. Mater. Chem. A* 6(13), 5234 (2018).
- A. Gadelmawla, K. Riess, J. Birkenstock, M. Hinterstein, K.G. Webber, and N.H. Khansur, Effect of varying Bi content on the temperature-dependent mechanical, dielectric, and structural properties of nominal Na_{1/2}Bi_{1/2}TiO₃. *J. Appl. Phys.* 130, 185106 (2021).
- T. Liu, H. Zhang, J. Zhou, A. Chang, and H. Jiang, Novel thermal-sensitive properties of NBT-BZT composites ceramics for high-temperature NTC thermistors. *J. Am. Ceram. Soc.* 103(1), 48 (2019).
- F. Li, J. Zhai, B. Shen, X. Liu, K. Yang, Y. Zhang, P. Li, B. Liu, and H. Zeng, Influence of structural evolution on energy storage properties in Bi_{0.5}Na_{0.5}TiO₃-SrTiO₃-NaNbO₃ lead-free ferroelectric ceramics. *J. Appl. Phys.* 121, 054103 (2017).
- H. Qi and R. Zuo, Linear-like lead-free relaxor antiferroelectric (Bi_{0.5}Na_{0.5})TiO₃-NaNbO₃ with giant energy-storage density/efficiency and super stability against temperature and frequency. *J. Mater. Chem. A* 7, 3971 (2019).
- M. Chandrasekhar, Y. Govinda Reddy, and P. Kumar, Dielectric, ferroelectric, and strain study of BNT-BT-BKT ceramics for actuator applications. *J. Electron. Mater.* 49, 7238 (2020).
- R. Kumari, N. Ahlawat, A. Agarwal, S. Sanghi, and M. Sindhu, Structural transformation and investigation of dielectric properties of Ca substituted (Na_{0.5}Bi_{0.5})_{0.95}-xBa_{0.05}Ca_xTiO₃ ceramics. *J. Alloys Compd.* 695, 3282 (2017).
- M. Acosta, J. Zang, W. Jo, and J. Rödel, High-temperature dielectrics in CaZrO₃-modified Bi_{1/2}Na_{1/2}TiO₃-based lead-free ceramics. *J. Eur. Ceram. Soc.* 32(16), 4327 (2012).
- C. Alemany, A.M. González, L. Pardo, B. Jimenez, F. Carmona, and J. Mendiola, Automatic determination of complex constants of piezoelectric lossy materials in the radial mode. *J. Phys. D: Appl. Phys.* 28(5), 945 (1995).
- Q. Xu, T. Li, H. Hao, S. Zhang, Z. Wang, M. Cao, Z. Yao, and H. Liu, Enhanced energy storage properties of NaNbO₃ modified

- Bi_{0.5}Na_{0.5}TiO₃ based ceramics. *J. Eur. Ceram. Soc.* 35(2), 545 (2015).
27. J. Zidani, M. Zannen, M. Hadouchi, H.A.H. Alzahrani, E. Birks, H. Khemakhem, M. Majdoub, M. El Marssi, and A. Lahmar, Structural, electrical and optical properties of lanthanide-doped Na_{0.4}K_{0.1}Bi_{0.5}TiO₃ ceramics. *Phys. B Condens. Matter* 653, 414680 (2023).
 28. M. Benyoussef, M. Zannen, J. Belhadi, B. Manoun, Z. Kutnjak, D. Vengust, M. Spreitzer, M. El Marssi, and A. Lahmar, Structural, dielectric, and ferroelectric properties of Na_{0.5}(Bi_{1-x}Nd_x)_{0.5}TiO₃ ceramics for energy storage and electrocaloric applications. *Ceram. Int.* 47(18), 26539 (2021).
 29. Y. Liu, Y. Lu, and S. Dai, Hydrothermal synthesis of monosized Bi_{0.5}Na_{0.5}TiO₃ spherical particles under low alkaline solution concentration. *J. Alloys Compd.* 484, 801 (2009).
 30. M. Vögler, N. Novak, F.H. Shader, and J. Rödel, Temperature-dependent volume fraction of polar nanoregions in lead-free (1-x)(Bi_{0.5}Na_{0.5})TiO₃-xBaTiO₃ ceramics. *Phys. Rev. B* 95, 024104 (2017).
 31. W. Jo, S. Schaab, E. Sapper, L.A. Schmitt, H.-J. Kleebe, A.J. Bell, and J. Rödel, On the phase identity and its thermal evolution of lead free (Bi_{1/2}Na_{1/2})TiO₃-6 mol% BaTiO₃. *J. Appl. Phys.* 110, 074106 (2011).
 32. D. Lin and K.W. Kwok, Structure, ferroelectric, and piezoelectric properties of (Bi_{0.5}Na_{0.5})_{1-x-y-z}(Bi_{0.5}K_{0.5})_xBa_ySr_zTiO₃ lead-free ceramics. *J. Am. Ceram. Soc.* 93(3), 806 (2010).
 33. A. Reyes-Montero, F. Rubio-Marcos, L.E. Fuentes-Cobas, A. Del Campo, R. Castañeda-Guzmán, M.E. Villafuerte-Castrejón, and L. Pardo, Confocal Raman microscopy, synchrotron X-ray diffraction, and photoacoustic study of Ba_{0.85}Ca_{0.15}Ti_{0.90}Zr_{0.10}O₃: understanding structural and microstructural response to the electric field. *ACS Appl. Electron. Mater.* 3(7), 2966 (2021).
 34. A. Reyes-Montero, L. Pardo, A. García, A.M. González, and M.E. Villafuerte-Castrejón, Ba_{1-x}Ca_xTi_{0.90}Zr_{0.10}O₃ shear properties and their frequency dependence determined from ceramic plates by an effective method for resonance decoupling. *J. Alloys Compd.* 806, 428 (2019).
 35. Q. Yao, F. Wang, C. Jin, Y. Tang, T. Wang, and W. Shi, Piezoelectric/photoluminescence effects in rare-earth doped lead-free ceramics. *Appl. Phys. A* 113, 231 (2013).
 36. J. Yang, P. Liu, X. Bian, H. Jing, Y. Wang, Y. Zhang, Y. Wu, and W. Song, Dielectric, ferroelectric and piezoelectric properties of Bi_{0.5}Na_{0.5}TiO₃-(Ba_{0.7}Ca_{0.3})TiO₃ ceramics at morphotropic phase boundary composition. *Mater. Sci. Eng. B* 176, 260 (2011).
 37. F. Yang, J.S. Dean, Q. Hu, P. Wu, E. Pradal-Velázquez, and D.C. Sinclair, From insulator to oxide-ion conductor by a synergistic effect from defect chemistry and microstructure: acceptor-doped Bi-excess sodium bismuth titanate Na_{0.5}Bi_{0.51}TiO_{3.015}. *J. Mater. Chem. A* 8, 25120 (2020).
 38. Y. An, C. He, C. Deng, Z. Chen, H. Chen, T. Wu, Y. Lu, X. Gu, J. Wang, Y. Liu, and Z. Li, Poling effect on optical and dielectric properties of Pr³⁺-doped Na_{0.5}Bi_{0.5}TiO₃ ferroelectric single crystal. *Ceram. Int.* 46(4), 4664 (2020).
 39. T. Yamatoh, H. Fujimori, and M. Arimura, Polymerizable complex synthesis of lead-free ferroelectric Na_{0.5}Bi_{0.5}TiO₃ suppressing evaporation of sodium and bismuth. *J. Ceram. Soc. Jpn.* 123, 978 (2015).

Publisher's Note Springer Nature remains neutral with regard to jurisdictional claims in published maps and institutional affiliations.